Proton Uptake in the Reaction Center Mutant L210DN from *Rhodobacter sphaeroides* via Protonated Water Molecules[†,‡]

Sabine Hermes, Joanna M. Stachnik, Delphine Onidas, André Remy, Eckhard Hofmann, and Klaus Gerwert*

Lehrstuhl für Biophysik, ND 04/596, Ruhr-Universität Bochum, D-44801 Bochum, Germany

Received April 18, 2006; Revised Manuscript Received September 8, 2006

ABSTRACT: The reaction center (RC) of *Rhodobacter sphaeroides* uses light energy to reduce and protonate a quinone molecule, Q_B (the secondary quinone electron acceptor), to form quinol, Q_BH_2. Asp210 in the L-subunit has been shown to be a catalytic residue in this process. Mutation of Asp210 to Asn leads to a deceleration of reoxidation of Q_A^- in the $Q_A^-Q_B \rightarrow Q_AQ_B^-$ transition. Here we determined the structure of the Asp210 to Asn mutant to 2.5 Å and show that there are no major structural differences as compared to the wild-type protein. We found Q_B in the distal position and a chain of water molecules between Asn210 and Q_B. Using time-resolved Fourier transform infrared (trFTIR) spectroscopy, we characterized the molecular reaction mechanism of this mutant. We found that Q_B^- formation precedes Q_A^- oxidation even more pronounced than in the wild-type reaction center. Continuum absorbance changes indicate deprotonation of a protonated water cluster, most likely of the water chain between Asn210 and Q_B. A detailed analysis of wild-type structures revealed a highly conserved water chain between Asp210 or Glu210 and Q_B in *Rb. sphaeroides* and *Rhodopseudomonas viridis*, respectively.

In photosynthetic bacteria the conversion of light energy into chemical energy is initiated within a protein called the reaction center (RC). The RC from *Rhodobacter sphaeroides* is a pigment-containing transmembrane protein complex of ~100 kDa. It represents one of the most studied bioenergetic model systems, both with respect to its structural characterization by crystallography (*1*) and with respect to the elucidation of its light-driven electron- and proton-transfer reactions (*2*).

Light induces the transfer of an electron from the primary donor, P,[1] which is a dimer of bacteriochlorophyll *a* molecules, via the intermediate acceptors bacteriochlorophyll *a* and bacteriopheophytin *a* to the primary acceptor quinone in the Q_A binding pocket and subsequently to the secondary quinone Q_B. The $P^+Q_A^-$ charge separation has been measured to occur within 200 ps (*3*), whereas the electron transition from Q_A^- to Q_B takes about 200 μs (*4*−*8*). The first electron transition from the primary to the secondary quinone is coupled to proton uptake from the cytoplasm (*4*, *9*). In the presence of an electron donor to P^+, the absorption of a second photon induces the double reduction and protonation of the secondary quinone and leads to the formation of Q_BH_2, which is released from the RC (*4*).

In 2003, Remy and Gerwert (*10*) proposed a new mechanistic view on the first electron transition from Q_A^- to Q_B, based on time-resolved step-scan FTIR measurements with a high time resolution down to 35 ns. They observed Q_B^- formation preceding Q_A^- oxidation. The clear separation of these two processes is permitted by the distinct bands in the IR of the two quinones Q_A and Q_B and semiquinones Q_A^- and Q_B^-, respectively (*11*−*13*). The assignment of the Q_A^- and Q_B^- bands in the IR is clear-cut, because specific isotopically labeled ubiquinones at the Q_A and Q_B positions shift clearly the bands at 1446 and 1479 cm^{-1}, respectively (*11*−*13*). In contrast, in the UV/VIS both bands overlap and a clear distiction between Q_A and Q_B absorbance changes is difficult. The observation in the IR led to the suggestion of an intermediary electron donor X, which reduces Q_B and is afterward rereduced by Q_A^-. A good candidate for the intermediary electron donor is the iron−histidine complex located between the Q_A and the Q_B pocket in the crystal structure (*14*). We recently ruled out the iron itself as the intermediary electron donor. Using time-resolved X-ray absorption spectroscopy (XAS), we did not observe a Fe^{II} to Fe^{III} transition during the light-induced reaction (*15*).

The proton uptake during the first electron transition seems to occur via a dedicated pathway. The entry point for the protons was identified to be at the surface of the H-subunit, near His126, His128, and Asp124, which bind metal ions such as Cd^{2+} and Zn^{2+} (*16*, *17*). Several amino acid residues between the proton entry region and the Q_B binding pocket have been proposed to form a proton transport pathway, based on the effects of site-directed mutagenesis, where protonatable groups were replaced with nonprotonatable ones (*18*−*20*). Asp17 in the M-subunit and Asp210 in the

[†] Financial support from the Deutsche Forschungsgemeinschaft by Grants SFB480-C3 and SFB480-C6 is gratefully acknowledged. D.O. gratefully acknowledges a fellowship by the Alexander von Humboldt foundation.

[‡] Atomic coordinates and related structure factors of the L210DN mutant reaction center have been deposited in the RCSB Protein Data Bank, Rutgers University, New Brunswick, NJ (PDB; http://www.rcsb.org/pdb/), accession number 2GMR.

* Corresponding author. Tel: +49 234 3224461. Fax: +49 234 3214238. E-mail: gerwert@bph.rub.de.

[1] Abbreviations: FTIR, Fourier transform infrared; P, primary electron donor; Q_A, ubiquinone at the primary acceptor binding site; Q_B, ubiquinone at the secondary acceptor binding site; X, intermediary electron donor; L210DN, aspartate 210 to asparagine mutation in the L-subunit; KIE, kinetic isotope effect.

10.1021/bi060742q CCC: $33.50
Published on Web 10/28/2006

L-subunit have been shown to be important elements in the proton transport chain. Replacement of these two residues by Asn in single and double mutants slowed the rate of proton transfer (*21*, *22*). Located near Q_B, the three residues Glu212, Ser223, and Asp213 in the L-subunit were shown to be crucial (reviewed in ref *4*). Mutation of Glu212 and Asp213 in the L-subunit to Asn did not alter tertiary structure (*23*, *24*). In addition, in the RC structures of *Rb. sphaeroides* (*1*) and *Rhodopseudomonas viridis* (*25*), a chain of ordered water molecules (up to 14 fixed water molecules) extending from the cytoplasm surface through the protein to Q_B was described. A more detailed water distribution in *Rps. viridis* showing a hydrogen-bonded network involving water molecules and amino acid side chains, which extends from the Q_B site to the cytoplasmic surface, was described thereafter in wild-type and mutant RCs and proposed to be relevant for proton uptake to Q_B (*26*, *27*).

In the L210DN mutant, the proton uptake pathway is disturbed, because no protonatable carboxyl group is available in this position. This slows down proton and electron transport. Here, we crystallized the protein and solved the structure at 2.5 Å resolution. We used the step-scan and rapid-scan FTIR techniques to characterize the molecular reaction mechanism of this mutant reaction center and present IR marker bands of the intermediary electron donor X. We present continuum absorbance changes in the IR, which are indicative of protonation changes in a protonated water cluster.

EXPERIMENTAL PROCEDURES

Purification. The *Rb. sphaeroides* reaction center mutant Asp210 to Asn in the L-subunit (L210DN) was constructed as described (*28*) and modified (*29*). Cells of the mutant were grown in PY medium (1% tryptone, 0.05% yeast extract, 2 mM $MgCl_2$, 2 mM $CaCl_2$, 0.001% $FeSO_4$) containing tetracycline (50 μg/mL) and kanamycin (12 μg/mL) for 3 days in the dark under semianaerobic conditions. Pelleted cells were resuspended in Tris buffer (10 mM Tris, 1 mM EDTA, 1 mM sodium azide, pH 8.0) containing 0.2 mM PMSF and disrupted by ultrasonification. The photosynthetic membranes were isolated from the supernatant by centrifugation, washed once, and homogenized in the Tris buffer. Reaction center membranes were solubilized in 1% lauryldimethylamine *N*-oxide (LDAO). The solubilized RC protein was further purified on a POROS HQ 50 (Applied Biosystems) column at 4 °C in Tris buffer/0.12% LDAO; elution was performed with increasing NaCl concentrations. The RC-containing fractions were pooled, diluted, and applied to a second POROS HQ 50 column. The RC solution was further purified by gel filtration on a High Load 16/60 Superdex 200 prep grade column equilibrated with 100 mM Tris, pH 8.0, 200 mM NaCl, and 0.12% LDAO. After gel filtration fractions with an absorbance ratio $A_{280}/A_{800} \leq 1.2$ were pooled and concentrated in a Vivaspin 30 concentration tube at 3000*g* to a final $OD_{800} = 20$.

Crystallization. Crystallization was achieved by the hanging-drop vapor diffusion method similar to reported protocols (see ref *30*) at 18 °C. 1,2,3-Heptanetriol [3% (w/v)] was added in solid form to the RC solution with $OD_{800} = 20$ and completely dissolved by vortexing. The suspension was mixed 1:1 (v/v) with a solution of 100 mM Tris, pH 8.0, 20% PEG4000, and 550 mM NaCl. Drops of 6 μL of mother solution were equilibrated against 700 μL of the reservoir solution consisting of 100 mM Tris, pH 8.0, 750 mM NaCl, and 20% PEG4000 at 18 °C. Thin, needle-shaped orthorhombic crystals, space group $P2_12_12_1$, appeared within 1−2 weeks. The crystals grew to 2 mm in length and to 0.1 mm for the other dimensions. RC L210DN crystals were mounted in Cryo-Loops, soaked in crystallization solution containing 10% (v/v) PEG400 as a cryoprotectant, and flash-cooled in liquid nitrogen. The obtained crystals had unit cell dimensions of $a = 76.85$ Å, $b = 134.72$ Å, and $c = 141.64$ Å. Crystallization was not well reproducible.

Table 1: Crystallographic Statistics for Data Collection and Refinement[a]

collection statistics	
beamline	SLS X10SA
resolution (Å)	38−2.5 (2.6−2.5)
space group	P 2_1 2_1 2_1
cell parameters (*a*, *b*, *c*) (Å)	76.85, 134.72, 141.64
wavelength (Å)	1.00
completeness (%)	97.4 (99.3)
multiplicity	6.5 (6.5)
average $I/\sigma I$	24.5 (6.4)
R_{sym} (%)	5.6 (33.4)
R_{meas}[b] (%)	6.1 (36.3)
R_{mrgd-F}[b] (%)	8.0 (27.8)
refinement statistics	
resolution (Å)	38−2.5
R_{cryst} (%)	21.2
R_{free}[c] (%)	24.7
average *B* factor (Å^2)	42.7
rmsd from ideality (protein atoms)	
bonds (Å)	0.007
angles (deg)	1.402
model	
no. of protein residues	825 (6477 atoms)
no. of cofactors	4 bacteriochlorophyll *a*, 2 bacteriopheophytin *a*, 2 ubiquinone, 1 spheroidenone, 1 iron (564 atoms total)
no. of waters	182 (182 atoms)
no. of detergents	4 lauryldimethylamine *N*-oxide (64 atoms)

[a] Data in parentheses represent values of the highest resolution bin. [b] For definition of R_{meas} and R_{mrgd-F}, see ref *31*. [c] R_{free} calculated from 5% of data omitted from refinement.

Data Collection and Analysis. Data to 2.5 Å were collected at the Swiss Light Source (SLS) at the X10SA station equipped with a Mar CCD detector. A single crystal was used to collect the entire data set at 100 K. Diffraction data were processed, merged, and scaled using the XDS program. The cell parameters, data collection, and final model statistics are given in Table 1. A total of 50281 unique reflections were recorded, giving data that were 97.4% complete between 38 and 2.5 Å, with an overall multiplicity of 6.5 and an overall R_{merge} of 8%.

Details of Model Building and Refinement. The structure was phased by molecular replacement using the program Molrep from the CCP4 package (*32*). The wild-type reaction center from *Rb. sphaeroides* [PDB code 1AIG (*14*)] determined at 2.6 Å was used as an initial model. The second RC molecule in the asymmetric unit cell (chains RSTD) and all water molecules were removed from the search structure. A rotation and translation search located one RC molecule in the asymmetric unit.

Rigid body refinement, calculation of electron density maps, simulated annealing, structural refinement, and temperature factor refinement were performed using CNS (*33*). The restraints used during refinement were as follows: The topology and parameter files of the software CNS (*33*) were used for the protein, ions, and water. The restraints for the reaction center cofactors were based on parameter and topology files from *Rps. viridis* [PDB entry code 1PRC (*26*)], which were modified. A new dictionary was made for spheroidenone. The ideal geometry values for the carotenoid were obtained from analysis of the Dundee PRODRG2 server (*34*).

Substitution of side chains, addition of water molecules, manual adjustment of the protein model, and rebuilding of the N- and C-terminal segments were performed using the software COOT from the CCP4 package (*32*).

The current model contains 825 residues and 10 bound cofactors with good stereochemistry. Only one residue, Asp82 of the H-chain, was found in the disallowed region of the Ramachandran plot. Tails of cofactors were not completely resolved for Q_A and Q_B due to missing or alternate electron density, and therefore the occupancy values were set to zero for atoms 41−56 (Q_A) and 24−56 (Q_B) before the last refinement. The average *B*-factor of the Q_B headgroup is 57.5 Å^2 and of the surrounding amino acid residues is 41.1 Å^2. Water molecules were considered if they had electron density in the $3F_o - 2F_c$ map contoured at 1.5σ and were within hydrogen-bonding distance to another water molecule or a protein atom. Additional water molecules were added manually to electron density with $\sigma > 1.0$ in the proximity of amino acid residues described as being involved in the formation of proton uptake pathways. Four LDAO molecules and one spheroidenone molecule could be reliably modeled in the electron density map and were included in the subsequent refinements.

Figures were produced using PYMOL (DeLano Scientific LLC, San Carlos, CA).

FTIR Measurements. The purified protein was concentrated using Vivaspin 500 concentrators (MWCO 30 kDa). Protein solution containing approximately 150 μg of RC (approximately 15 μL) was pipetted onto a CaF window and concentrated under a gentle nitrogen stream to 1 μL. The window was sealed with a second one and mounted into a metal cuvette. Q_B^- activity was checked at 960 nm and measured as ~80%. Samples for measurements where the primary donor was immediately rereduced after the start of the electron-transfer cycle were prepared in a similar way: after partial concentrating, the reaction center was covered with a solution containing 10 mM sodium ascorbate and 20 mM 2,3,5,6-tetramethyl-*p*-phenylenediamine (DAD), and the mixture was concentrated to 1 μL. FTIR measurements were taken in an IFS 88 or IFS 66v (Bruker) at 278 K. The reaction was started by an eximer-pumped dye laser (532 nm, 30 ns, ~5 mJ). Ten (5) time-resolved interferogram recordings were directly averaged in a single rapid-scan run. Each sample relaxed for 48 s (230 s) to ensure full recombination. Single rapid-scan runs were started at different times after the laser flash (0, 1, 2, 3, 4, 5, 8, 13, 19, 25 ms). Thirty runs (12 runs) with a complete series of starting times were averaged for the presented data, i.e., 300 measurements (60 measurements) of four (three) different samples. Numbers are given for samples without P^+-reducing agent and in brackets for samples including P^+-reducing agent.

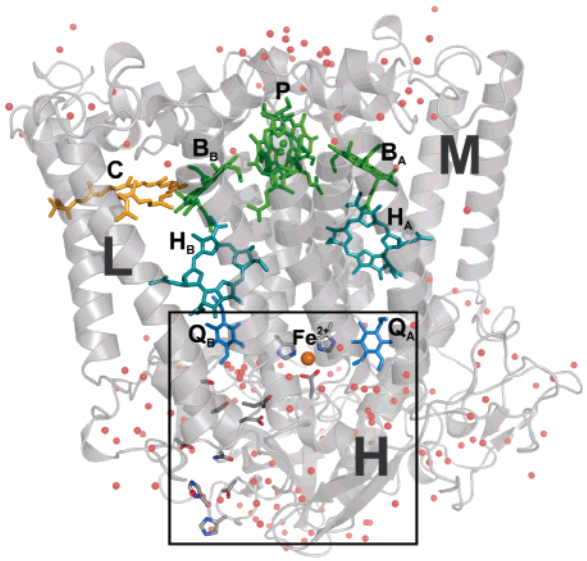

FIGURE 1: Overall structure of the crystallized L210DN mutant reaction center. Main chains L, M, and H are shown as gray cartoons, and cofactors are represented as sticks. Key: green, bacteriochlorophyll *a* (P, special pair; B_A and B_B, accessory bacteriochlorophylls); cyan, bacteriopheophytin *a* (H_A and H_B); blue, quinone (Q_A and Q_B); orange, spheroidenone. Amino acid residues of the iron−histidine complex and the proton uptake channel are represented as gray sticks with red for oxygen atoms and blue for nitrogen atoms. Water molecules are depicted as red spheres. The iron is shown as an orange sphere. The framed region is shown in detail in Figure 8.

The step-scan FTIR measurements were carried out as described previously (*10*). Static light-induced FTIR difference spectra were obtained using a Fiberoptic-Heim LQ 2600 lamp for illumination. $P^+Q_A^-/PQ_A$, $P^+Q_B^-/PQ_B$, Q_A^-/Q_A, and Q_B^-/Q_B spectra were respectively recorded at 123, 278, 263, and 298 K and a light intensity of 90, 90, 90, and 15 W. Samples for measurements without Q_B were prepared following the same protocol as for samples containing P^+-reducing agent. In addition, they were covered with a 15 mM terbutryn in ethanol solution and concentrated to 1 μL.

Hydrogen/deuterium (H/D) exchange measurements were performed as described in ref *35*. Measurements were taken at 278 K. To separate the bands of interest from those caused by water vapor in the sample, a protein-free reference spectrum was subtracted from the experimental data.

Fitting Procedure. All data were analyzed by the Global fit method including all wave numbers from 1900 to 950 cm^{-1} (*36*).

RESULTS

Integrity of the Asp210 to Asn Mutant Protein. Figure 1 shows an overview of the L210DN reaction center structure with a cartoon representation of the main protein chains, cofactors, and selected amino acid residues of the iron−histidine center and the proton uptake pathway. The structure has been refined to an *R* factor of 21.3% (R_{free} = 24.6%) at a resolution of 2.5 Å (Table 1). Comparison of the backbone of our crystal structure with that of the L, M, and H chain of the wild-type structure 1AIJ [2.2 Å (*14*)] showed a high congruence (rmsd of 0.323 Å). The side chain structure was

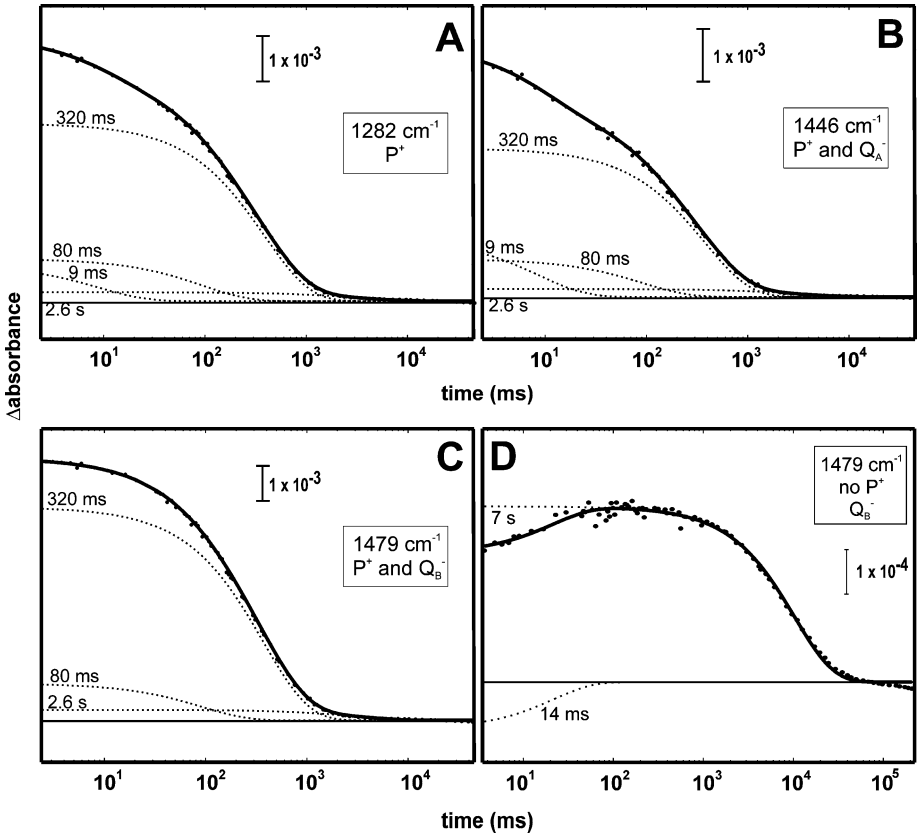

FIGURE 2: Infrared absorbance changes of marker bands for special pair P^+ and semiquinones Q_A^- and Q_B^- in the Asp210 to Asn mutant of the photosynthetic reaction center. Data are shown as dots; bold lines describe the global fit and dotted lines display the partial contribution of the fit components, times given relate to half-times of the respective reaction. (A−C) Untreated protein sample. Rates of 320 ms and 2.6 s are assigned to $P^+Q_B^-/PQ_B$ recombination, the rate of 80 ms is assigned to $P^+Q_A^-/PQ_A$ recombination, the rate of 9 ms is assigned to the $Q_A^-X^+/Q_AX$ transition. (D) Sodium ascorbate/DAD-treated samples to reduce P^+. The rate of 7 s is assigned to $Q_A^-Q_B^-$ recombination with the redox mediator, and the rate of 14 ms is assigned to the $Q_A^-X^+/Q_AX$ transition.

very similar to that of the wild-type reaction center 1AIJ. The differences are mainly due to regions that show only weak or missing electron density. These regions, chain H, residues 79−81, and the termini of the protein chains, are located on the surface of the protein and therefore are very mobile. The position of the cofactors is very similar to that of the wild-type structure 1AIJ (*14*). Q_B is found in the distal position. Reliable electron density was observed for the headgroup of Q_B only in this position, which is illustrated in the omit map (see Figure S1 in the Supporting Information). An occupancy of the proximal position can be ruled out. The distribution of water molecules was found to be similar to that of wild-type structures. For some water positions present in wild-type structures we did not model water molecules due to weak or missing electron density. At these positions in the mutant, it is highly probable that water molecules are very mobile and are therefore not resolved. We did not find water molecules at positions not previously modeled in wild-type structures. No alternative path of hydrogen-bonded amino acid residues and water molecules was observed in the mutant. However, the resolution of the structural data has to be improved to obtain a more detailed picture of water molecules in this reaction center mutant.

Static Q_B^-/Q_B spectra of the L210DN mutant (not shown) do not differ significantly from the published data (*19*, *37*). Q_A^-/Q_A spectra correspond to our own wild-type spectra (not shown). The high degree of congruence between wild-type and mutant spectra again rules out larger structural alterations in the mutant protein. As the crystallographic results lead to the same conclusion, both methods confirm each other regarding the integrity of the mutant protein.

Time-Resolved Measurements of the Asp210 to Asn Mutant Reaction Center. The Asp210 to Asn mutant exhibited a decelerated rate for the proposed Q_A^- to X^+ transition (*10*). Therefore, this process can be resolved by the experimentally much less demanding rapid-scan FTIR technique.

At 1282 cm^{-1} the P^+ decay can be observed (*38*) (Figure 2A). The absorbance change is described by four apparent time constants: 9 ms, 80 ms, 320 ms, and 2.6 s. For each time constant an amplitude spectrum can be obtained. As the static difference spectra, it describes the absorbance changes involved in the respective transition. The three slower time constants are assigned to $P^+Q_A^-/PQ_A$ (80 ms) and $P^+Q_B^-/PQ_B$ (320 ms, 2.6 s) recombination, because the amplitude spectra agree nicely with the respective static difference spectra of the charge-separated states. Therefore, the band assignments performed in the static difference spectra can also be used for the time-resolved amplitude spectra. The additional 9 ms time constant in the kinetic description of this P^+ marker band is surprising and was not observed in the wild type. Obviously, part of the P^+/P recombination process starts already at this early time point in the Asp210 to Asn mutant reaction center. Figure 2B shows the absorbance change at a marker band for Q_A^-, which is overlapped with the P^+ absorbance change. Here the absorbance change was described by the same three recombination time constants caused by P^+ (80 ms, 320 ms,

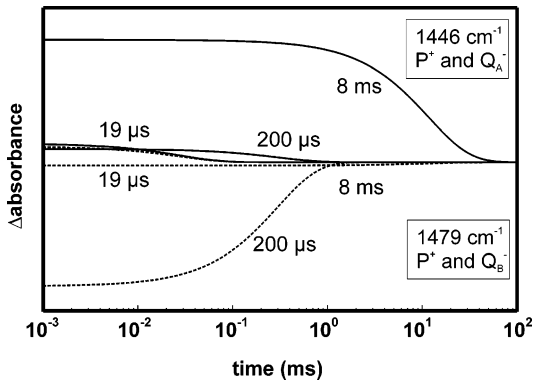

FIGURE 3: Partial fit components of early events in the light-induced reactions of Q_A^- and Q_B^- in the Asp210 to Asn mutant of the photosynthetic reaction center. Continuous lines describe the early absorbance changes at 1446 cm^{-1} for Q_A^-, and dotted lines describe the early absorbance changes at 1479 cm^{-1} for Q_B^-. Q_B^- formation takes place at mainly 200 μs, whereas Q_A^- oxidation occurs later at mainly 8 ms.

and 2.6 s). The 9 ms time constant has approximately double the amplitude relative to the 80 ms amplitude, as compared to the kinetics of P^+ at 1282 cm^{-1}. Therefore, we assign the additional part of this time constant to the electron transition from Q_A^- to the intermediate X^+ (see below). Figure 2C shows the absorbance change at the marker band for Q_B^- overlapped with P^+. It was described by the three recombination time constants of P^+ alone. If the electron transition would proceed directly from Q_A^- to Q_B, the absorbance change of Q_B^- at 1479 cm^{-1} should increase with 9 ms, the same rate at which Q_A^- disappears. This is not observed in Figure 2C. Because the P^+ absorbance overlays the Q_B^- absorbance, we conducted additional rapid-scan measurements with eliminated P^+ signals, where the primary donor was immediately rereduced after the actinic flash. At 1479 cm^{-1}, these measurements actually do not show an appearance of Q_B^- with 9 ms as would be expected for a direct Q_A^- to Q_B electron transfer. The small residual increase of Q_B^- absorbance at 14 ms (Figure 2D) is due to back-reactions. Obviously, the reaction is slightly decelerated from 9 to 14 ms in the presence of the redox mediators. The observed apparent rate constants depend on forward and backward reactions, in contrast to intrinsic rate constants describing single reaction steps. Such small contribution due to back-reactions was also observed in wild type (*10*). Nevertheless, if Q_A^- would directly transfer an electron to Q_B, Q_B should appear with 9 ms (or 14 ms), which is obviously not the case. This rules out a direct Q_A^- to Q_B transition in the L210DN mutant as in wild type, and an intermediary electron donor must be involved.

Early Events of the Q_A to Q_B Transition. In order to resolve the reduction of Q_B, a better time resolution is needed. Therefore, step-scan measurements with 35 ns time resolution were performed. A step-scan experiment of the L210DN mutant reaction center resolves the early events of the electron transition from Q_A to Q_B. Figure 3 shows, only in the time range of interest, the Q_A^- and Q_B^- marker bands at 1446 and 1479 cm^{-1}, respectively. At 1479 cm^{-1} the main signal increases with 200 μs. This absorbance increase represents the reduction of Q_B. The other time constants, 19 μs and 8 ms, have very low amplitudes and do not significantly improve the kinetic description. At 1446 cm^{-1}, the 8 ms time constant describes oxidation of Q_A^- in

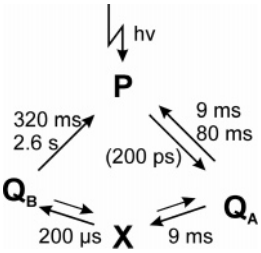

FIGURE 4: Scheme of light-induced reactions and their apparent rates in the Asp210 to Asn mutant of the photosynthetic reaction center. The figure shows the electron-transfer reactions in the reaction center samples as determined in this study by time-resolved measurements.

agreement to the 9 ms time constant observed in the rapid-scan experiment (Figure 2B). The 19 and 200 μs time constants play a subordinate role in the kinetic description. As was observed for the wild-type reaction center, the electron-transfer reactions proceed asynchronously. In this mutant the separation of both processes is even more pronounced. The findings confirm that Q_B^- formation occurs prior to Q_A^- oxidation, and an intermediary redox component must be involved.

As a summary of the measurements, a reaction scheme of the reaction center mutant L210DN is presented in Figure 4. It shows the electron transition steps and time constants assigned to the different processes, including the recombination time constants for $P^+Q_A^-/PQ_A$ (80 ms) and $P^+Q_B^-/PQ_B$ (320 ms, 2.6 s), as well as time constants for the electron transition from the proposed intermediary electron donor X to Q_B (200 μs) and from Q_A^- to X^+ (9 ms). We admit that at present it is hard to understand why X should be oxidized before Q_A is reduced, but the experimental results are obvious.

Protonation Events during Electron Transition. In ref *10* protonation events in the wild-type reaction center were monitored at 1751 and 1724 cm^{-1}: 1724 cm^{-1} was assigned to protonated Glu212 in the L-subunit (*19*); 1751 cm^{-1} was tentatively assigned to protonated Asp210 in the L-subunit (*10*). However, it could not be conclusively ruled out that Asp17 in the M-subunit might be responsible for the observed absorbance changes (*10*). The band at 1751 cm^{-1} showed that a carboxyl group, most probably Asp210 in the L-subunit, was protonated at 12 and 150 μs and deprotonated at 1.1 ms (Figure 5A), whereas Glu212 at 1724 cm^{-1} was protonated at 1.1 ms and deprotonated during recombination (not shown). It was therefore concluded that Asp210 protonates Glu212.

The protonation signal at 1751 cm^{-1} should be absent in the Asp210 to Asn mutant. In the wild-type reaction center, this band increased by 12 and 150 μs, whereas in the mutant only a decrease is observed (Figure 5B). In order to show that the residual absorbance change of the mutant protein at 1751 cm^{-1} (in Figure 5B) is due to P^+/P recombination, measurements on the mutant with reduced primary donor P were performed. With reduced primary donor no absorbance change at this wave number is observed (Figure 5C). Therefore, the band at 1751 cm^{-1} is now clearly assigned to protonation of Asp210 in the L-subunit.

Figure 5D shows the protonation of Glu212 at 1724 cm^{-1} from rapid-scan measurements of the L210DN mutant reaction center with reduced primary donor. Glu212 becomes

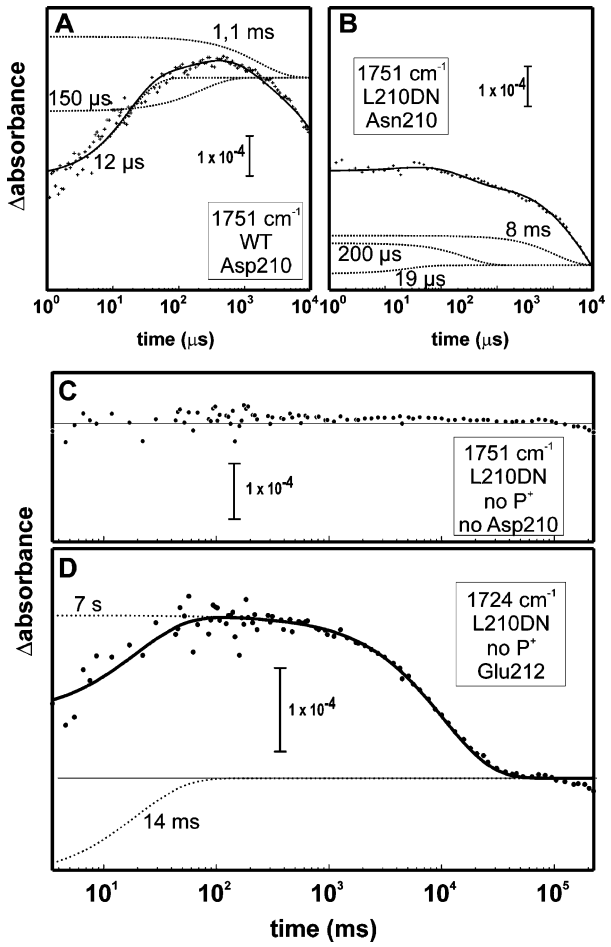

FIGURE 5: Infrared absorbance changes of marker bands for Asp210 in the L-subunit in the wild type and in the Asp210 to Asn mutant of the photosynthetic reaction center. Absorbance change data are shown as crosses or dots; bold lines describe the global fit, and dotted lines display the partial contribution of the fit components. (A) In the wild-type reaction center Asp210 is protonated mainly at 12 and 150 μs and deprotonated at 1.1 ms. (B) In the Asp210 to Asn mutant reaction center, no protonation can be observed, as no protonatable group is present (from ref *10*). (C) In the mutant reaction center measured in the presence of a P^+ reducing agent, no absorbance change is observed at 1751 cm^{-1}. (D) In the mutant reaction center measured in the presence of a P^+ reducing agent, protonation of Glu212 is observed at 14 ms.

protonated at 14 ms and an additional faster, but not resolved, time component. Evidently, the proton transfer proceeds via an alternative pathway in the mutant; it might involve Asp17 in the M-subunit (*21*, *22*) or bound water molecules.

Assignments of Bands to the Intermediary Electron Donor. By comparison of the 9 ms amplitude spectrum (representing $P^+Q_A^-X^+$ to PQ_AX) to the 80 ms amplitude spectrum (representing $P^+Q_A^-$ to PQ_A) of the Asp210 to Asn mutant (Figure 6A), we should be able to assign bands to the intermediary electron donor in its reduced (X) and its oxidized state (X^+), respectively. The amplitude spectrum at 80 ms agrees with the static spectrum of $P^+Q_A^-/PQ_A$. According to the scheme in Figure 4, the 9 ms time constant describes the electron transition from Q_A^- to the oxidized intermediary electron donor X^+. In addition, at this rate $P^+Q_A^-$ to PQ_A recombination is already partly taking place in the mutant. Therefore, the 9 ms time constant describes a mixed $Q_A^-X^+$ to Q_AX and $P^+Q_A^-$ to PQ_A transition, whereas the 80 ms time constant describes a $P^+Q_A^-$ to PQ_A transition.

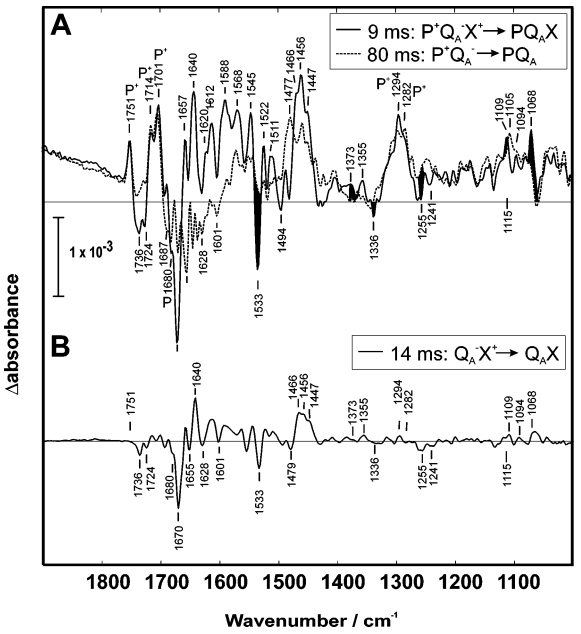

FIGURE 6: (A) Comparison of the 9 and 80 ms amplitude spectra of the Asp210 to Asn mutant of the photosynthetic reaction center. The 9 ms amplitude spectrum is shown as a continuous line, and the 80 ms amplitude spectrum is shown as a dotted line. Bands are labeled with their respective wave numbers. Filled bands are explained in the text. (B) Amplitude spectra of the $Q_A^-X^+$ to Q_AX transition in the Asp210 to Asn mutant of the photosynthetic reaction center. Contributions of the primary donor P/P^+ are eliminated.

Both amplitude spectra contain about the same strength of signals for the P^+ to P transition, as can be observed for the main P^+ bands as marked. Due to baseline shifts under the strong amide and water bands deviations between 1700 and 1500 cm^{-1} were not further regarded. Bands not assigned to P/P^+ recombination have to be considered as $Q_A^-X^+/Q_AX$ bands in the 9 ms amplitude spectrum. Strong Q_A bands at 1670 cm^{-1} (*39*) and Q_A^- bands at 1466 and 1446 cm^{-1} (*11*) indicate Q_A^- oxidation to Q_A in this process. Bands which do not belong to P^+/P or Q_A^-/Q_A should be caused by the X^+/X transition. These are a strong negative (−) band at 1533 cm^{-1} and a strong positive band (+) at 1068 cm^{-1}. In addition, bands at 1109 cm^{-1} (+), 1255 cm^{-1} (−), 1336 cm^{-1} (−), and 1373 cm^{-1} (+) might be assigned to X or X^+. These bands were also observed in the corresponding spectrum of measurements with reduced primary donor. In these measurements, the corresponding amplitude spectrum lacks the specific P^+/P bands (Figure 6B). It therefore represents a $Q_A^-X^+$ to Q_AX difference spectrum.

Protonated Water Clusters in the RC Mutant. Broad continuum bands in the spectral region of 3000−2000 cm^{-1} are a signature of protonated hydrogen-bonded water networks within proteins (*35*, *40*). Broad absorbance changes in the RC have been observed (see ref *41*) in static difference spectra. However, broad absorbance changes can also be caused by baseline drifts, which often occur during long measuring times to obtain static spectra. Therefore, we performed time-resolved FTIR measurements to assign clear-cut continuum absorbance changes. For the first time we identified in time-resolved IR measurements in the RC continuum absorbance changes for the Q_A^- to X and the Q_B^- to Q_B transition (Figure 7). The different maxima indicate different sizes of the protonated water complex, e.g., an Eigen

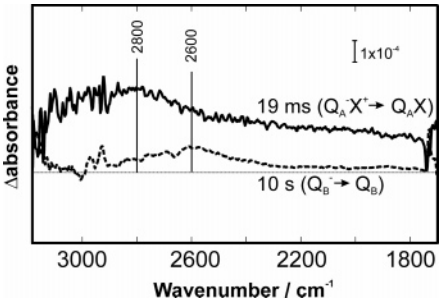

FIGURE 7: Time-resolved observation of changes in a protonated water cluster. Amplitude spectra of continuum absorbance changes at 19 ms of the $Q_A^-X^+$ to Q_AX transition (solid line) and at 10 s of the Q_B^- to Q_B transition (dashed line) between 3200 and 1700 cm^{-1}. Approximate maxima are labeled.

cluster ($H_9O_4^+$) or a Zundel cluster ($H_5O_2^+$) (*42*). The bands in the amplitude spectra indicate a deprotonation of a protonated water cluster.

In addition, we measured an H/D exchange spectrum of the L210DN mutant in the ground state and observed a band at 3681 cm^{-1} in H_2O and 2719 cm^{-1} in D_2O, which is evidence for a dangling OH group, i.e., a not hydrogen-bonded OH group (preliminary result).

DISCUSSION

The time-resolved FTIR measurements of the Asp210 to Asn mutant in the L-subunit of the reaction center lead to a description with three time constants for the $Q_A^-Q_B$ to $Q_AQ_B^-$ transition (19 μs, 200 μs, and 9 ms) and three recombination time constants (80, 320, and 2.6 ms). Noticeably, in contrast to the wild-type protein, we observed that partial $P^+Q_A^-$/PQ_A recombination already occurred at 9 ms. In addition, we observed that the first time constant for the $P^+Q_B^-$/PQ_B recombination was 2.4 times faster than in wild type (320 ms compared to 770 ms) in agreement with UV/VIS measurements (*22*). Evidently, the changed electrostatic environment in the mutant during the $P^+Q_B^-$ state provides less stabilization to the semiquinone Q_B^-, and therefore the lifetime of this state is decreased.

This mutant had been previously investigated by time-resolved UV/VIS and FTIR measurements. However, FTIR measurements using the rapid-scan technique with 25 ms time resolution were not able to resolve the intermediate or protonation changes of Asp210 in the L-subunit (*43*). UV/VIS measurements at 750 nm are sensitive to reduction states of both Q_A^- and Q_B^- (*44*, *45*), and absorbance changes were described only with a single-exponential fit, although according to the authors, a better fit could be obtained with a sum of two exponentials (*21*, *22*). Comparison with wild-type (*10*) data revealed that the third time constant of the $Q_A^-Q_B$ to $Q_AQ_B^-$ transition in the mutant undergoes an approximately 8-fold deceleration (1.1 ms in the wild type, 9 ms in the L210DN mutant). An 8-fold reduction of the overall reaction time constant was also observed in UV/VIS measurements (*22*).

It is striking that in the Asp210 to Asn mutant selectively the 1.1 ms rate is slowed. The question arises as to why a mutation in the proton pathway to Q_B leads to an approximately 8-fold deceleration of the reoxidation of Q_A^- compared to the wild type. It is also observed that alone the reduction of Q_A is enough to induce cytoplasmic proton uptake (*46*). These findings indicate a close coupling between the proton uptake and the oxidation of Q_A, which had also been implied from theoretical calculations on the *Rps. viridis* RC (*47*). Evidently, the slow Q_A^- reoxidation is dependent on proton movement in the proton uptake pathway. In contrast, the main portion of Q_B reduction takes place at a similar time constant in mutant and wild-type reaction center (200 and 150 μs, respectively). Therefore, we conclude that reduction of Q_B is not dependent on proton transfer in the proton uptake channel, whereas protonation of Glu212 in the L-subunit is coupled to the reoxidation of Q_A^-.

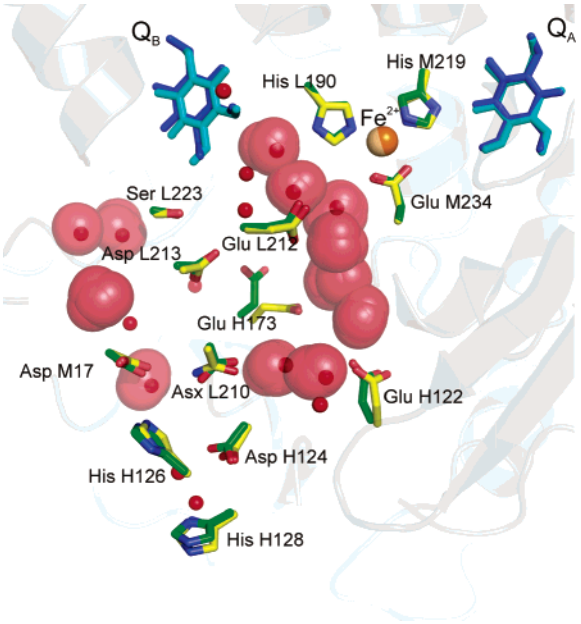

FIGURE 8: Structural details of the water channel in the Asp210 to Asn mutant of the photosynthetic reaction center. Selected amino acid residues are shown of the structure 1AIJ in green and of the L210DN structure in yellow. The iron is shown as an orange (1AIJ) or beige (L210DN) sphere. Small red spheres depict water molecules modeled into our structure (displayed are only waters within 5 Å distance of the shown amino acid residues). The large red spheres represent the consensus water molecules from the wild-type structures 1AIJ, 1DS8, 1JGY, 1K6L, 1M3X, 1OGV, 1PCR, and 2BNP. Structure files of 1AIJ and 1DS8 each contain two molecules; in these cases water molecules from both molecules were considered. Cartoon representation of the protein in gray is from the L210DN structure.

The different kinetic isotope effects (KIE) for Glu212 protonation in D_2O for the wild type (KIE = 4.9; not shown) and the L210DN mutant (KIE = 1.3; not shown) suggest a varying mechanism of proton transfer in the two species. If the rotational rearrangement of a water molecule is rate-limiting for proton transfer, a KIE of $\sqrt{2}$ is observed, reflecting the mass ratio between proton and deuteron (*48*). This seems to be the case in the Asp210 to Asn mutant reaction center, where Asp210, as the proton donor to Glu212, is missing. In this case, the proton might instead be donated from a protonated water molecule. If the proton displacement within the H bond is rate-limiting, much greater KIEs are reported (*48*, *49*). This is probably the case in the wild-type reaction center, where a proton bound to Asp210 has to be released from the carboxyl group to be transferred to Glu212. The structural data support this view (Figure 8). In wild-type reaction centers of *Rb. sphaeroides* a chain of conserved water molecules with hydrogen-bonding distance can be found between Asp210 and Glu212 in the L-subunit,

including the carboxyl group of Glu122 in the H-subunit. The homologous residue Asp125 in *Rps. viridis* had been described also to be part of a hydrogen-bonded cluster of strongly interacting amino acid residues in the proximity of the Q_B binding pocket (*26*, *47*). Recently, Glu122 in *Rb. sphaeroides* was also suggested to be part of a delocalized proton transport network (*50*). Comparison with *Rps. viridis* structures (*26*, *27*) revealed a similar conserved distribution of water molecules in this part of the structure. Water molecules that are modeled into most structures can be assumed to be tightly bound to the protein and are also expected to be present in newly crystallized structures. In the mutant no water molecules between Glu122 in the H-subunit and Glu212 in the L-subunit can be resolved. If the same path was used in the mutant, protonated water molecules would have to move inside the channel in order to donate the proton to Glu212.

In bacteriorhodopsin it was recently shown how the interplay between a strong hydrogen-bonded water molecule, a dangling water, and a protonated water complex transfers a proton from the Schiff base, the central proton binding site, to the external medium (*40*). Here, we also identified such dangling water and a protonated water complex changing its size during the Q_A to Q_B transition. Therefore, we propose that in a very similar mechanism as in bacteriorhodopsin a proton is transferred from Asp210 to Glu212 via a chain of water molecules. Further experiments have to be performed to obtain such a detailed mechanism as found in bacteriorhodopsin.

Further work will be carried out to assign the identified absorbance bands of the intermediary electron donor to a specific molecular group. This study of the Asp210 to Asn mutant in the L-subunit of the reaction center shows that the protein complex is functional and structurally intact. However, due to the slowed electron-transfer reaction from Q_A^- to X^+, it is accessible to the rapid-scan FTIR technique.

ACKNOWLEDGMENT

We thank Gabriele Smuda for technical assistance in protein production and purification. Part of this work was performed at the Swiss Light Source, Beamline X10SA, Paul Scherrer Institute, Villigen, Switzerland. We especially acknowledge the help of the beamline staff during data collection.

SUPPORTING INFORMATION AVAILABLE

An additional figure showing the electron density and the modeled structure in the proximity of Q_B. This material is available free of charge via the Internet at http://pubs.acs.org.

REFERENCES

1. Ermler, U., Fritzsch, G., Buchanan, S. K., and Michel, H. (1994) Structure of the photosynthetic reaction centre from *Rhodobacter sphaeroides* at 2.65 Å resolution: cofactors and protein-cofactor interactions, *Structure 2*, 925−936.
2. Wraight, C. A. (2004) Proton and electron transfer in the acceptor quinone complex of photosynthetic reaction centers from *Rhodobacter spaeroides*, *Front. Biosci. 9*, 309−337.
3. Holzapfel, W., Finkele, U., Kaiser, W., Oesterhelt, D., Scheer, H., Stilz, H. U., and Zinth, W. (1990) Initial electron-transfer in the reaction center from *Rhodobacter sphaeroides*, *Proc. Natl. Acad. Sci. U.S.A. 87*, 5168−5172.
4. Okamura, M. V., Paddock, M. L., Graige, M. S., and Feher, G. (2000) Proton and electron transfer in bacterial reaction centers, *Biochim. Biophys. Acta 1458*, 148−163.
5. Tiede, D. M., Vazquez, J., Cordova, J., and Marone, P. A. (1996) Time-resolved electrochromism associated with the formation of quinone anions in the *Rhodobacter sphaeroides* R26 reaction center, *Biochemistry 35*, 10763−10775.
6. Graige, M. S., Feher, G., and Okamura, M. Y. (1998) Conformational gating of the electron transfer reaction $Q_A^{-\bullet}Q_B \rightarrow Q_AQ_B^{-\bullet}$ in bacterial reaction centers of *Rhodobacter sphaeroides* determined by a driving force assay, *Proc. Natl. Acad. Sci. U.S.A. 95*, 11679−11684.
7. Li, J., Gilroy, D., Tiede, D. M., and Gunner, M. R. (1998) Kinetic phases in the electron transfer from $P^+Q_A^-Q_B$ to $P^+Q_AQ_B^-$ and the associated processes in *Rhodobacter sphaeroides* R-26 reaction centers, *Biochemistry 37*, 2818−2829.
8. Li, J., Takahashi, E., and Gunner, M. R. (2000) $-\Delta G$(AB) and pH dependence of the electron transfer from $P^+Q_A^-Q_B$ to $P^+Q_AQ_B^-$ in *Rhodobacter sphaeroides* reaction centers, *Biochemistry 39*, 7445−7454.
9. Paddock, M. L., Feher, G., and Okamura, M. Y. (2003) Proton transfer pathways and mechanism in bacterial reaction centers, *FEBS Lett. 555*, 45−50.
10. Remy, A., and Gerwert, K. (2003) Coupling of light-induced electron transfer to proton uptake in photosynthesis, *Nat. Struct. Biol. 10*, 637−644.
11. Brudler, R., de Groot, H. J. M., van Liemt, W. B. S., Steggerda, W. F., Esmijer, R., Gast, P., Hoff, A. J., Lugtenburg, J., and Gerwert, K. (1994) Asymmetric binding of the 1- and 4-C═O groups of Q_A in *Rhodobacter sphaeroides* R26 reaction centres monitored by Fourier transform infra-red spectroscopy using site-specific isotopically labelled ubiquinone-10, *EMBO J. 13*, 5523−5530.
12. Brudler, R., de Groot, H. J. M., van Liemt, W. B. S., Gast, P., Hoff, A. J., Lugtenburg, J., and Gerwert, K. (1995) FTIR spectroscopy shows weak symmetric hydrogen bonding of the QB carbonyl groups in *Rhodobacter sphaeroides* R26 reaction centres, *FEBS Lett. 370*, 88−92.
13. Breton, J., Boullais, C., Burie, J., Nabedryk, E., and Mioskowski, C. (1994) Binding sites of quinones in photosynthetic bacterial reaction centers investigated by light-induced FTIR difference spectroscopy: Assignment of the interactions of each carbonyl of QA in *Rhodobacter sphaeroides* using site-specific ^{13}C-labeled ubiquinone, *Biochemistry 33*, 14378−14386.
14. Stowell, M. H., McPhillips, T. M., Rees, D. C., Soltis, S. M., Abresch, E., and Feher, G. (1997) Light-induced structural changes in photosynthetic reaction center: implications for mechanism of electron-proton transfer, *Science 276*, 812−816.
15. Hermes, S., Bremm, O., Garczarek, F., Derrien, V., Liebisch, P., Loja, P., Sebban, P., Gerwert, K., and Haumann, M. (2006) A time-resolved iron-specific X-ray absorption experiment yields no evidence for an $Fe^{2+} \rightarrow Fe^{3+}$ transition during $Q_A^- \rightarrow Q_B$ electron transfer in the photosynthetic reaction center, *Biochemistry 45*, 353−359.
16. Paddock, M. L., Graige, M. S., Feher, G., and Okamura, M. Y. (1999) Identification of the proton pathway in bacterial reaction centers: inhibition of proton transfer by binding of Zn^{2+} or Cd^{2+}, *Proc. Natl. Acad. Sci. U.S.A. 96*, 6183−6188.
17. Axelrod, H. L., Abresch, E. C., Paddock, M. L., Okamura, M. Y., and Feher, G. (2000) Determination of the binding sites of the proton transfer inhibitors Cd^{2+} and Zn^{2+} in bacterial reaction centers, *Proc. Natl. Acad. Sci. U.S.A. 97*, 1542−1547.
18. Okamura, M. Y., and Feher, G. (1992) Proton transfer in reaction centers from photosynthetic bacteria, *Annu. Rev. Biochem. 61*, 861−896.
19. Nabedryk, E., Breton, J., Hienerwadel, R., Fogel, C., Mäntele, W., Paddock, M. L., and Okamura, M. Y. (1995) Fourier transforms infrared difference spectroscopy of secondary quinone acceptor photoreduction in proton transfer mutants of *Rhodobacter sphaeroides*, *Biochemistry 34*, 14722−14732.
20. Takahashi, E., and Wraight, C. A. (1992) Proton and electron transfer in the acceptor quinone complex of *Rhodobacter sphaeroides* reaction centers: characterization of site-directed mutants of the two ionizable residues, GluL212 and AspL213, in the Q_B binding site, *Biochemistry 31*, 855−866.
21. Paddock, M. L., Feher, G., and Okamura, M. Y. (2000) Identification of the proton pathway in bacterial reaction centers: replacement of Asp-M17 and Asp-L210 with asn reduces the proton

transfer rate in the presence of Cd^{2+}, *Proc. Natl. Acad. Sci. U.S.A. 97*, 1548−1553.
22. Paddock, M. L., Ädelroth, P., Chang, C., Abresch, E. C., Feher, G., and Okamura, M. Y. (2001) Identification of the proton pathway in bacterial reaction centers: cooperation between Asp-M17 and Asp-L210 facilitates proton transfer to the secondary quinone (Q_B), *Biochemistry 40*, 6893−6902.
23. Chirino, A. J., Lous, E. J., Huber, M., Allen, J. P., Schenck, C. C., Paddock, M. L., Feher, G., and Rees, D. C. (1994) Crystallographic analyses of site-directed mutants of the photosynthetic reaction center from *Rhodobacter sphaeroides*, *Biochemistry 33*, 4584−4593.
24. Xu, Q., Axelrod, H. L., Abresch, E. C., Paddock, M. L., Okamura, M. Y., and Feher, G. (2004) X-ray structure determination of three mutants of the bacterial photosynthetic reaction centers from *Rb. sphaeroides*; Altered proton transfer pathways, *Structure 12*, 703−715.
25. Deisenhofer, J., Epp, O., Sinning, I., and Michel, H. (1995) Crystallographic refinement at 2.3 Å resolution and refined model of the photosynthetic reaction centre from *Rhodopseudomonas viridis*, *J. Mol. Biol. 246*, 429−457.
26. Lancaster, C. R. D., and Michel, H. (1997) The coupling of light-induced electron transfer and proton uptake as derived from crystal structures of reaction centres from *Rhodopseudomonas viridis* modified at the binding site of the secondary quinone, Q_B, *Structure 5*, 1339−1359.
27. Lancaster, C. R., Bibikova, M. V., Sabatino, P., Oesterhelt, D., and Michel, H. (2000) Structural basis of the drastically increased initial electron transfer rate in the reaction center from a *Rhodopseudomonas viridis* mutant described at 2.00-Å resolution, *J. Biol. Chem. 275*, 39364−39368.
28. Farchaus, J. W., and Oesterhelt, D. (1989) A *Rhodobacter sphaeroides* puf L, M and X deletion mutant and its complementation in trans with a 5.3 kb puf operon shuttle fragment, *EMBO J. 8*, 47−54.
29. Remy, A. (2002) Der $Q_A^-Q_B \rightarrow Q_AQ_B^-$ Übergang im bakteriellen photosynthetischen Reaktionszentrum von *Rhodobacter sphaeroides*, Thesis Ruhr-University Bochum, Bochum, Germany.
30. Fritzsch, G. (1998) Obtaining crystal structures from bacterial photosynthetic reaction centers, *Methods Enzymol. 297*, 57−77.
31. Diederichs, K., and Karplus, P. A. (1997) Improved R-factors for diffraction data analysis in macromolecular crystallography, *Nat. Struct. Biol. 4*, 269−275.
32. Collaborative Computational Project, Number 4 (1994) The CCP4 Suite: Programs for Protein Crystallography', *Acta Crystallogr. D50*, 760−763.
33. Crystallography and NMR System (1998) *Acta Crystallogr. D54*, 905−921.
34. Schuettelkopf, A. W., and van Aalten, D. M. F. (2004) PRODRG—a tool for high-throughput crystallography of protein-ligand complexes, *Acta Crystallogr. D60*, 1355−1363.
35. Garczarek, F., Brown, L. S., Lanyi, J. K., and Gerwert, K. (2005) Proton binding within a membrane protein by a protonated water cluster, *Proc. Natl. Acad. Sci. U.S.A. 102*, 3633−3638.
36. Hessling, B., Souvignier, G., and Gerwert, K. (1993) A model-independent approach to assigning bacteriorhodopsin's intramolecular reactions to photocycle intermediates, *Biophys. J. 65*, 1929−1941.
37. Nabedryk, E., Breton, J., Okamura, M. Y., and Paddock, M. L. (2001) Simultaneous replacement of Asp-L210 and Asp-M17 with Asn increases proton uptake by Glu-L212 upon first electron transfer to Q_B in reaction centers from *Rhodobacter sphaeroides*, *Biochemistry 40*, 13826−13832.
38. Mäntele, W. G., Wollenweber, A. M., Nabedryk, E., and Breton, J. (1988) Infrared spectroelectrochemistry of bacteriochlorophylls and bacteriopheophytins: Implictations for the binding of the pigments in the reaction center from photosynthetic bacteria, *Proc. Natl. Acad. Sci. U.S.A. 85*, 8468−8472.
39. Thibodeau, D. L., Nabedryk, E., Hienerwadel, R., Lenz, F., Mäntele, W., and Breton, J. (1990) Time-resolved FTIR spectroscopy of quinones in *Rb. sphaeroides* reaction centers, *Biochim. Biophys. Acta 1020*, 253−259.
40. Garczarek, F., and Gerwert, K. (2006) Functional waters in intraprotein proton transfer monitored by FTIR difference spectroscopy, *Nature 439*, 109−112.
41. Breton, J., and Nabedryk, E. (1998) Proton uptake upon quinone reduction in bacterial reaction centers: IR signature and possible participation of a highly polarizable hydrogen bond network, *Photosynth. Res. 55*, 301−307.
42. Headrick, J. M., Diken, E. G., Walters, R. S., Hammer, N. I., Christie, R. A., Cui, J., Myshakin, E. M., Duncan, M. A., Johnson, M. A., and Jordan, K. D. (2005) Spectral signatures of hydrated proton vibrations in water clusters, *Science 308*, 1765−1769.
43. Mezzetti, A., Nabedryk, E., Breton, J., Okamura, M. Y., Paddock, M. L., Giacometti, G., and Leibl, W. (2002) Rapid-scan Fourier transform infrared spectroscopy shows coupling of GLu-L212 protonation and electron transfer to Q_B in *Rhodobacter sphaeroides* reaction centers, *Biochim. Biophys. Acta 1553*, 320−330.
44. Vermeglio, A., and Clayton, R. K. (1977) Kinetics of electron transfer between the primary and the secondary electron acceptor in reaction centers from *Rhodopseudomonas sphaeroides*, *Biochim. Biophys. Acta 461*, 159−165.
45. Kleinfeld, D., Okamura, M. Y., and Feher, G. (1984) Electron transfer in reaction centers of *Rhodopseudomonas sphaeroides*. I. Determination of the charge recombination pathway of $D^+Q_AQ^-_B$ and free energy and kinetic relations between $Q^-_AQ_B$ and $Q_AQ^-_B$, *Biochim. Biophys. Acta 766*, 126−140.
46. Maroti, P., and Wraight, C. A. (1997) Kinetics of H^+ ion binding by the $P^+Q_A^-$ state of bacterial photosynthetic reaction centers: rate limitation within the protein, *Biophys. J. 73*, 367−381.
47. Lancaster, C. R. D., Michel, H., Honig, B., and Gunner, M. R. (1996) Calculated coupling of electron and proton transfer in the photosynthetic reaction center of *Rhodopseudomonas viridis*, *Biophys. J. 70*, 2469−2492.
48. Eigen, M. (1963) Protonenübertragung, Säure-Base-Katalyse und enzymatische Hydrolyse, Teil I: Elementarvorgänge, *Angew. Chem. 75*, 489−508.
49. Agmon, N. (1995) The Grotthuss mechanism, *Chem. Phys. Lett. 244*, 456−62.
50. Ishikita, H., and Knapp, E. W. (2005) Energetics of proton transfer pathways in reaction centers from *Rhodobacter sphaeroides*, *J. Biol. Chem. 280*, 12446−12450.

BI060742Q